NANO LETTERS

pubs.acs.org/NanoLett Letter

Multiterminal Inverse AC Josephson Effect

Ethan G. Arnault,* Trevyn F. Q. Larson, Andrew Seredinski, Lingfei Zhao, Sara Idris, Aeron McConnell, Kenji Watanabe, Takashi Taniguchi, Ivan Borzenets, François Amet, and Gleb Finkelstein

Cite This: *Nano Lett.* 2021, 21, 9668−9674 Read Online

ACCESS | Metrics & More | Article Recommendations | Supporting Information

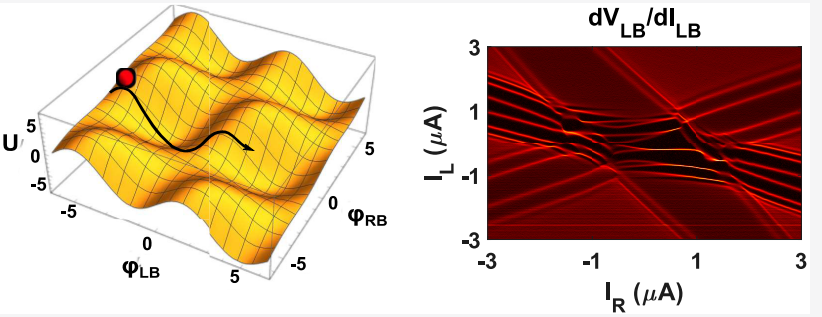

ABSTRACT: When a Josephson junction is exposed to microwave radiation, it undergoes the inverse AC Josephson effect—the phase of the junction locks to the drive frequency. As a result, the $I-V$ curves of the junction acquire "Shapiro steps" of quantized voltage. If the junction has three or more superconducting contacts, coupling between different pairs of terminals must be taken into account and the state of the junction evolves in a phase space of higher dimensionality. Here, we study the multiterminal inverse AC Josephson effect in a graphene sample with three superconducting terminals. We observe robust fractional Shapiro steps and correlated switching events, which can only be explained by considering the device as a completely connected Josephson network. We successfully simulate the observed behaviors using a modified two-dimensional RCSJ model. Our results suggest that multiterminal Josephson junctions are a playground to study highly connected nonlinear networks with novel topologies.

KEYWORDS: *AC Josephson Effect, Shapiro Steps, Topological Materials, Superconductivity, Driven-Dissipative Systems*

INTRODUCTION

The superconducting phase of a resistively and capacitively shunted Josephson junction (JJ) has the same dynamical properties as a pendulum.[1,2] This endows Josephson junctions with a rich phenomenology at the confluence of nonlinear and quantum dynamics.[3] Networks of JJs in particular offer the opportunity to design a highly tunable nonlinear oscillator in arbitrary dimension. Indeed, Josephson arrays have been shown to host not only a variety of quantum states, but also nonlinear dynamical behaviors such as synchronization,[4] chimera states,[5] splay states,[6,7] and chaos.[8]

While Josephson arrays have been studied extensively (see, e.g., refs 9−11), the phase dynamics of driven multiterminal Josephson junctions have yet to be fully explored. In multiterminal junctions, a Josephson coupling is established between each pair of superconducting contacts across a common normal channel (for instance, graphene). An electron microscope image of such a device is shown on Figure 1a in the three terminal case. The added complexity makes multiterminal junctions an ideal medium for engineering novel quantum and topological phenomena. For example, the energy spectrum of multiterminal Josephson junction based on a few-mode semiconductor has been predicted to emulate the band structure of topologically nontrivial materials.[12−21] This exciting prospect led to renewed efforts toward experimental realizations of multiterminal Josephson junctions,[22−28] which calls for new insights into their phase dynamics.

An important step in characterizing junction dynamics is exploring the evolution of the superconducting phase under a microwave excitation.[29] In a conventional two terminal Josephson junction, the junction phase could lock to the phase of the external drive. This results in Shapiro steps: the rectification of the applied microwave current which generates a quantized DC voltage across the junction $V = \frac{\hbar}{2e}\left\langle \frac{d\phi}{dt} \right\rangle$ at integer or fractional multiples of $V = \frac{\hbar\omega}{2e}$, where ω is the drive frequency.[30] The phase locking is well understood in the context of the Stewart−McCumber (RCSJ) model, whereby an imaginary phase particle rolls down the rungs of a tilted

Received: September 8, 2021
Revised: November 10, 2021
Published: November 15, 2021

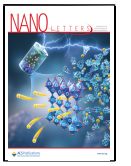

https://doi.org/10.1021/acs.nanolett.1c03474
Nano Lett. 2021, 21, 9668−9674

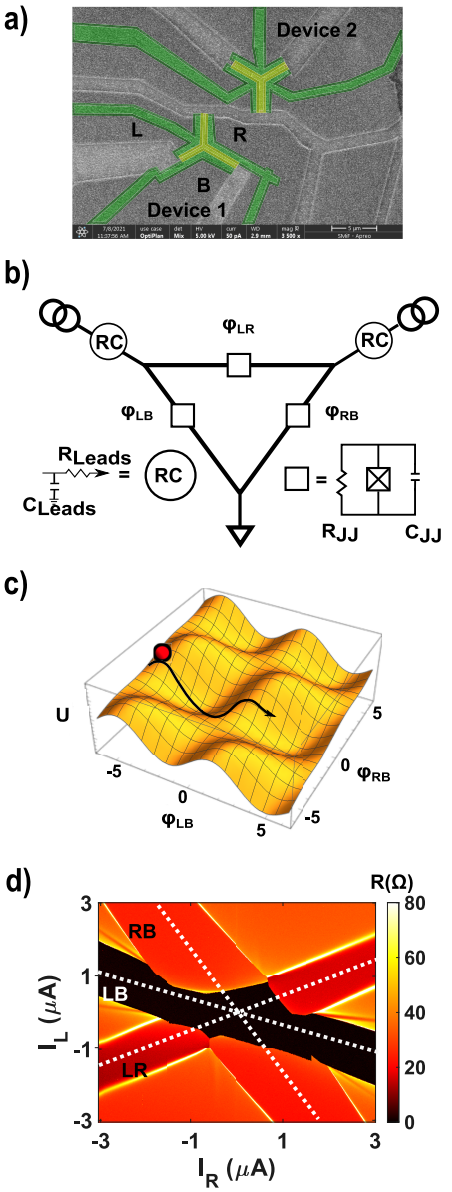

Figure 1. (a) SEM image of the studied device. A 500 nm channel of monolayer graphene is contacted by three MoRe leads of widths between 6.5 and 7.5 μm. Current I_L is sourced from **L** and I_R from **R**. **B** is grounded. Voltages are measured between each contact and ground. (b) Circuit model of the device. All three superconducting contacts are connected via Josephson junctions, resistors, and capacitors. (c) Illustration of the trajectory of the phase particle through the two-dimensional washboard potential. (d) Differential resistance (dV_{LB}/dI_L) bias–bias map at zero microwave power and V_g = 10 V. The three branches corresponds to supercurrent between three pairs of contacts.

washboard potential.[10] Since the washboard potential is determined by the junction's current–phase relationship (CPR), Shapiro steps can serve as a probe into the CPR, which is especially useful for studying Josephson junctions made from unconventional materials.[31−36]

The state of the three-terminal junction is described by two independent phases, e.g. the phases of the left (**L**) and right (**R**) terminals with respect to the grounded bottom (**B**) terminal (Figure 1a,b). The two phase differences ϕ_{LB} and ϕ_{RB} encode a washboard potential, as illustrated on Figure 1c and detailed in the Supporting Information. The applied DC currents tilt the washboard potential in a certain direction, while an AC excitation generates a rocking motion. In a general case, the AC currents applied to the two contacts could differ both in amplitude and in phase. The resulting out-of-phase rocking of the washboard potential along each axis therefore tends to push the phase along elliptical trajectories, which become open, drifting spirals if DC biases are superimposed to the periodic drive.

In this paper, we unravel the phase dynamics of a three-terminal Josephson junction under microwave irradiation. In this case, mode-locking can occur both between the drive and the two phases ϕ_{LB} and ϕ_{RB}, as well as between the two phases themselves due to their coupling. Indeed, we observe signatures of collective behaviors, such as fractional phase locking and oscillator synchronization. We qualitatively model the system with a multiterminal generalization of the conventional RCSJ model.[10]

RESULTS

Our multiterminal junction consists of monolayer graphene encapsulated in hexagonal boron nitride, which protects the device from fabrication contaminants and enables ballistic transport over several microns,[37,38] including ballistic supercurrents.[39−41] The junction's three contacts are made of sputtered molybdenum–rhenium (MoRe), a superconductor known to form high transparency Ohmic contacts to graphene.[40] The primary device studied here is Y-shaped, with the three junctions meeting at a 120 degree angle (Figure 1a). The contacts are separated by a 0.5 μm long graphene channel, and the junctions widths (lateral extent of the contacts) range between 6.5 and 7.5 μm. Fabrication details are provided in the Supporting Information.

The sample is cooled to a base temperature of 50 mK in a Leiden Cryogenics dilution refrigerator. However, additional heating from the microwave signal can warm the sample holder to several hundred mK. In fact, it has been reported that in similar microwave-driven superconductor–normal–superconductor (SNS) junctions the actual electron temperature may be even higher.[35] Unless otherwise stated, we apply 10 V to the back gate, which corresponds to an electron density of 2.5 × 10^{12}/cm^2. A small magnetic field offset of 0.5 mT is used to suppress the critical current of the junctions. This allows us to tune between different nonlinear regimes and suppress hysteresis in our Shapiro steps.[3,42] In the Supporting Information, we present two representative results measured at zero field and at a different gate voltages.

In the typical measurement, DC bias currents I_L and I_R are applied to the **L** and **R** contacts with respect to the grounded **B** contact. We present either the DC voltages V_{LB} and V_{RB} or the low-frequency differential resistances dV_{LB}/dI_L and dV_{RB}/dI_R (measured using a lock-in amplifier). In Figure 1d, we plot dV_{LB}/dI_L vs I_L and I_R, measured without applied microwave radiation. The resulting map is consistent with previous studies by us and other groups.[25−27] Three superconducting branches emerge corresponding to supercurrents flowing between each pair of contacts. Additional "quartet" features emerge between the branches,[22,24] which will not be the focus of this study.

We now send a 5.2 GHz signal to an antenna located ∼1 mm from the device. The microwave excitation applied at room temperature by the signal generator passes through several attenuators, reducing the power reaching the sample by at least 5 orders of magnitude. Since the delivered power varies as a function of frequency, we quote only the power applied by

https://doi.org/10.1021/acs.nanolett.1c03474
Nano Lett. 2021, 21, 9668−9674

the signal generator. In Figure 2, we apply 15 dBm of microwave power and measure the voltages of each junction.

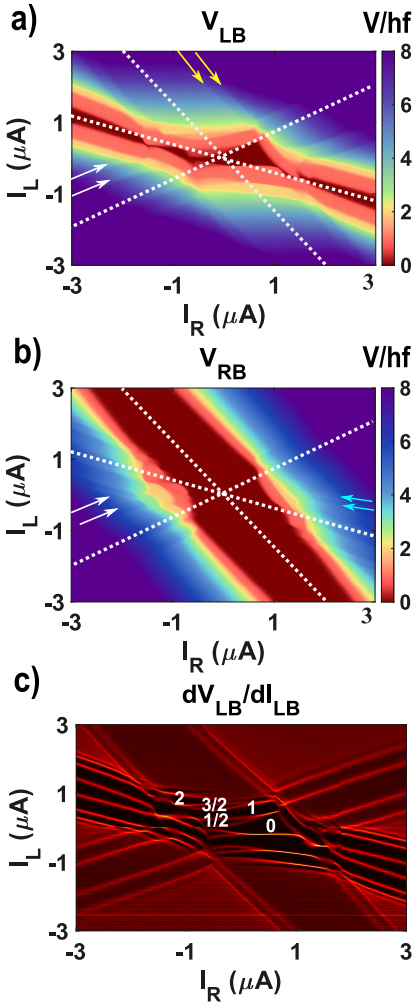

Figure 2. DC voltage maps for junctions *LB* (a) and *RB* (b) at 5.2 GHz, 15 dBm, and V_{bg} = 10 V. White dashed lines indicate the biasing conditions which result in zero voltage across one of the three junctions. At high bias, imprints of other junctions emerge as ripples on each map parallel to the white dashed lines (arrows mark the location of the ripples, cyan from *LB*, yellow from *RB*, white from *RL*). (c) Differential map of panel a to highlight the plateau boundaries. Half integer Shapiro steps emerge in the *LB* (and *LR*) junction at the intersection of the ripples induced by the *RB* junction. These half integer steps disappear for high applied biases, where only the single junction behavior is present.

As a guide to the eye, we add dashed white lines, which correspond to contours of constant voltage across all three Josephson junctions *RB*, *LB*, and *LR*, as extracted from Figure 1d (measured in the absence of the microwave excitation).

When a sufficiently large current bias is applied to a given contact, the corresponding phase is not locked to the drive and its voltage with respect to ground is not quantized. However, another junction in the network may simultaneously exhibit Shapiro steps, which couple to the measured junction through the device's circuit network and cause voltage ripples. For instance, note the ripples in V_{LB} marked by yellow arrows in Figure 2a, which are parallel to the lines of constant V_{RB} in Figure 2b. This feature corresponds to the imprint of junction *RB* onto junction *LB*. In a similar fashion, the imprint of *LB* on *RB* is observed in Figure 2b (shown by cyan arrows); imprints from *LR* (not shown) are observed in both maps (shown by white arrows).

Figure 2c highlights the step boundaries by showing the numerical derivative of the *LB* voltage map. Here, at the intersection of all three voltage branches, the junctions' mutual influence become even more pronounced, resulting in the appearance of prominent half integer steps. Depending on the parameters, the half integer steps are observed between any pair of contacts (see the Supporting Information).

To elucidate the origin of the half integer steps, we consider several observations: (1) Upon increasing the bias out of the central region ($I_{L,R}$ < 1 μA), only integer steps remain—the half integer steps have disappeared. (2) The half steps are washed away at about the same temperature as the integer steps (see the Supporting Information). (3) In the previous measurements of individual graphene junctions of similar dimension, which used the same experimental setup, we have not observed such prominent fractional steps as in Figure 2.[42] As we argue further in the text, these three observations indicate that the origin of the fractional steps is not due to typical single junction considerations, such as nonsinusoidality in the CPR[43−48] or the circuit components external to the junction such as a capacitor or inductive load.[49,50] Instead, the most likely origin of the observed behavior is the multiterminal nature of the present sample. Indeed, it has been predicted that Josephson networks could demonstrate fractional steps due to the full breadth of their circuitry, even when their constituent junctions have sinusoidal CPR.[51]

To understand the origin of the half-integer plateaus, we have to consider spiraling trajectories in a two-dimensional washboard potential of Figure 1c. These trajectories can cause the phase to land on a saddle point of the washboard potential after a cycle of the drive, rather than a global minimum. It then could take more than one cycle to reach the global minimum, which yields fractional voltage plateaus. This intuitive picture is substantiated by the numerical simulations in Figure 4c,d, which we describe later in more detail. Here, the two-dimensional washboard is tilted horizontally by I_L, while I_R = 0. The resulting rocking motion in the ϕ_R direction keeps V_R = 0 on average. However, the trajectory spirals down along the ϕ_L direction, progressing by 2π every two cycles. As a result, a substantial half frequency subharmonic of the applied microwave excitation is generated. The rectification of this $\omega/2$ frequency results in fractional Shapiro steps with $V_L = 1/2\,\frac{\hbar\omega}{2e}$.

We next turn our attention to the evolution of the Shapiro steps with the power of the microwave signal. In Figure 3, I_L is swept, while I_R is tuned to ∼−300 nA, which is the offset bias best suited to capture both the 1/2 and 3/2 steps (see Figure 2c). To better identify the plateau boundaries, we take a numerical differential of Figure 3a with respect to I_L (Figure 3b).

Two observations are immediately visible in Figure 3a,b:

First, it is notable that the integer and fractional steps have comparable widths. Shapiro steps at fractional multiples of $\hbar\omega/2e$ can appear in a single junction with either a sinusoidal[49,50] or a nonsinusoidal[43−48] current−phase relation. However, those fractional steps are typically much less robust than their integer counterparts. On the other hand, frustrated Josephson arrays have demonstrated integer and fractional plateaus of similar widths,[52] indicating that network effects in

https://doi.org/10.1021/acs.nanolett.1c03474
Nano Lett. 2021, 21, 9668−9674

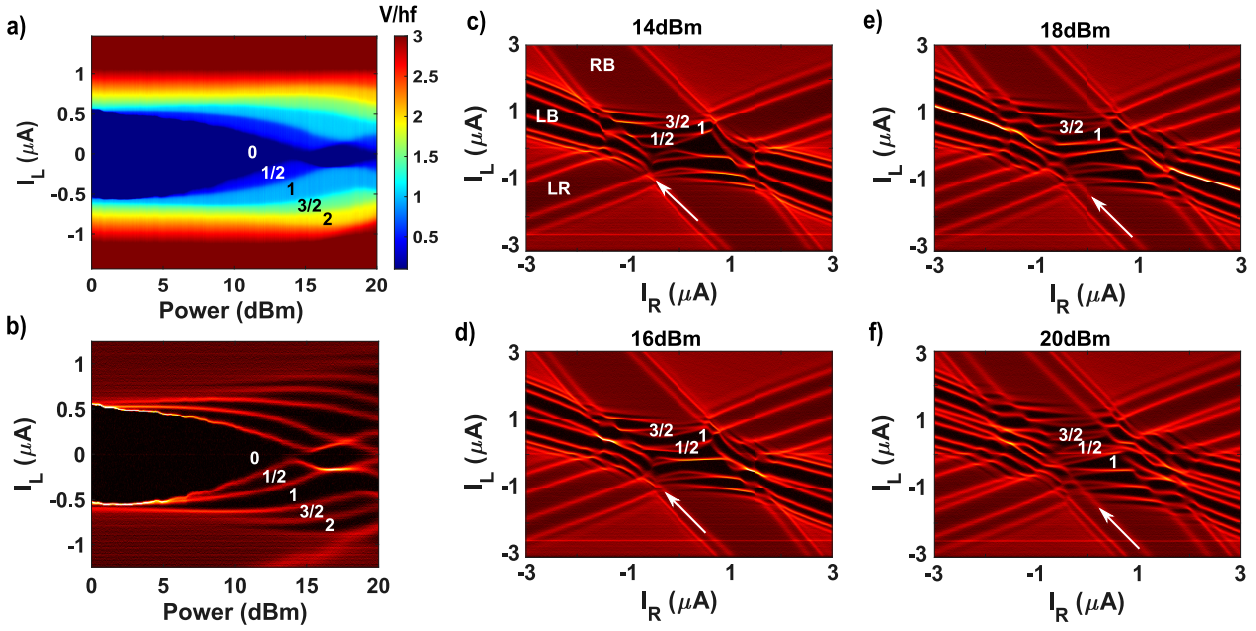

Figure 3. (a) V_{LB} at fixed I_R = −300 nA while varying I_L and applied microwave power. The Shapiro steps demonstrate the prototypical Bessel function behavior, including the half-integer steps. Notably, the step width of of the fractions is comparable to the width of the integer steps. (b) Numerical derivative of a as a guide to the eye. (c−f) Differential bias−bias maps tracking the evolution of the plateaus with changing microwave power. At the boundary generated by the *RB* ± 1 step, the fractional plateaus are forced to switch (denoted by white arrows).

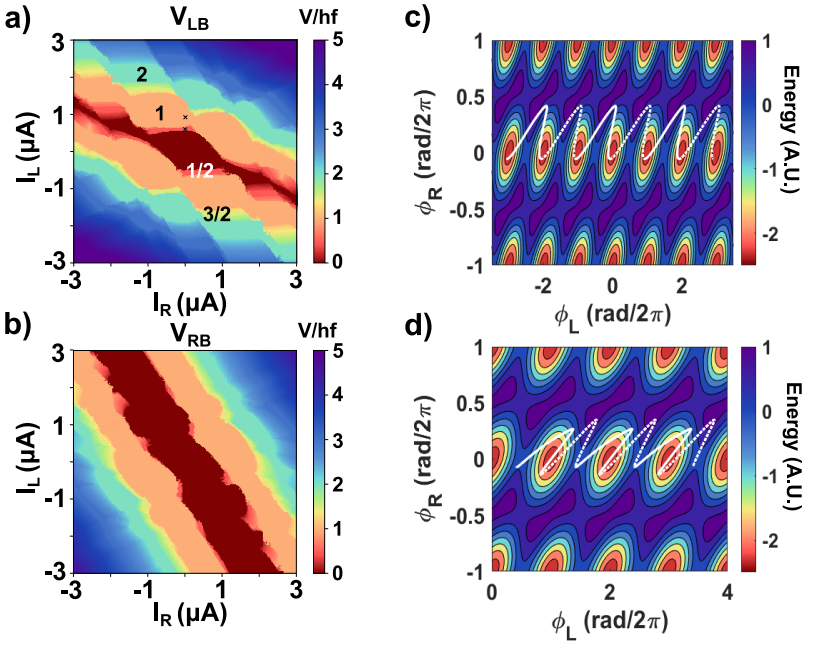

Figure 4. (a,b) Simulated bias−bias maps of the *LB* (a) and *RB* (b) junctions. Our simulation produces comparable results to the experiment, capturing both the general shape of the plateaus as well as the fractional steps. Simulation parameters are listed in the Supporting Information. X's mark the location in bias where the phase trajectories are taken. (c,d) Phase trajectory of the 1 (c) and 1/2 (d) plateaus overlaid atop the energy landscape. Alternating dashed and solid lines correspond to one cycle of the drive. A slow rocking motion develops within the minima. The rocking allows the phase particle to avoid global maxima and run across the diagonal of the potential. This causes a stable cycling finishing near global minima for integers. Meanwhile, trajectories that end near both minima and saddle points generate fractional steps.

connected Josephson junctions are universally more robust in comparison to individual device dynamics.

Second, both the fractional and the integer steps in Figure 3a,b all show qualitatively the same behavior as the integer steps in a prototypical single junction.[10] There, the plateau widths are described by $IJ_n\left(\frac{2eV_{AC}}{\hbar\omega}\right)$, where J_n is the Bessel function, which appears to be very similar to Figure 3. (See, e.g., our results in ref 42.) We are not aware of a simple argument why the half-integer steps in our case would follow the same type of pattern. Moreover, our previous measurements of a single graphene junction of similar dimensions showed strong deviations from the Bessel functions.[42] Instead, large overlap between plateaus resulted in pronounced

https://doi.org/10.1021/acs.nanolett.1c03474
Nano Lett. 2021, 21, 9668−9674

hysteresis which modified the shape of the plateaus. In the Supporting Information, we show that when the multiterminal junction is tuned into the hysteretic regime, the fractional plateaus disappear, being overwhelmed by the integer steps.

The formation of both integer and fractional plateaus is made clear through the study of the bias−bias maps at various microwave powers (Figures 3c−e). At high bias, each junction develops it is own set of integer Shapiro steps. At the same time, in the central region, where the superconducting branches meet, a complicated web of integer and fractional plateaus is formed.

Focusing on the ±1/2 steps, we note that the plateaus are interrupted upon reaching the *RB* junction's ±1 boundary, which itself is nearly unaffected. (The *RB* boundary is denoted by the white arrows.) This observation demonstrates that the stability of the fractional steps is weaker than that of the integer steps. We argue that the fractional phase trajectory is critically disrupted by the transition to a running state of the *RB* junction which traverses multiple periods of ϕ_{RB}. It is important to note that the variations in dynamical states of the junctions, which fundamentally change the phase trajectory, are more disruptive than the temperature fluctuations for the temperature ranges studied.

To link our experimental findings and theoretical understanding, we now turn to modeling the dynamics of the multiterminal junction. We use a fourth order Runge−Kutta method to solve a series of coupled differential equations derived from the multiterminal generalization of the RCSJ model, schematically shown in Figure 1b. More details, as well as a list of parameters used in the simulation are found in the Supporting Information.

Modeling the behavior of Figure 2, we find good qualitative agreement between the simulation and the experiment, capturing both the fractional steps as well as the general shape of the plateaus (Figure 4a,b). The simulations also produce the trajectory of the phase "particle" in the $\phi_{L,R}$ space. Figure 4c,d depicts the simulated phase evolution taken at biases corresponding to the V_{LB} = 1 and 1/2 plateaus respectively, while V_{RB} = 0. The trajectories are overlaid atop the energy landscape. In the ϕ_R direction, the particle is rocking back and forth to keep $\left\langle \frac{d\phi_R}{dt} \right\rangle = 0$. Thus, one full cycle of the drive corresponds to ϕ_R returning back to the same value. The rocking allows for the "particle" to climb over regions lower than the typical maxima. The less steep path allows for the particle to traverse several minima in the ϕ_L direction before ultimately returning to the same point, shifted n periods away. It is suggestive that, for integers, these trajectories seem to end on minima (Figure 4c), while, for fractions (Figure 4d), trajectories seem to end on either minima or saddle points. The quasistability of the saddle point may explain why the fractional steps are more dynamically sensitive than the integer steps.

DISCUSSION

In conclusion, we study the Shapiro steps in a multiterminal Josephson junction made of graphene, which provides all possible connections between pairs of superconducting terminals. The interplay within the full network of couplings allows for the generation of robust fractional Shapiro steps and correlated transitions between junctions. The multijunction origin of the fractional steps separates itself from typically observed fractions, which are usually born from the single junction CPR or external circuitry. Further, the fractional plateaus are found to be more sensitive to changes in dynamical state than the integer plateaus, despite having comparable sensitivity to temperature. These findings are simulated using an extended RCSJ model, where it is shown that the fractional plateaus emerge due to nontrivial phase trajectories across the 2D washboard potential.

It is important to emphasize that our model does not include the possibility of Andreev reflections coupling all three contacts. These processes should be present only in the central region of the sample, and hence should be suppressed in our geometry which is dominated by long junctions coupling individual pairs of contacts. Correspondingly, we model our sample as a plaquette of three independent Josephson junctions. The overwhelming similarity of the simulations and the measurements must be considered in future works so as not to confuse the rich physics of the multiterminal Andreev scattering with the physics of the circuit network itself.

In the future, adding more contacts will provide unique circuit topologies that are not realizable in two-dimensional Josephson arrays. This may enable experimental observations of chimera[5] and splay states,[6,7] which are predicted in Josephson arrays, but with the added benefit of being able to bias or measure from any junction directly. Additionally, making junctions from novel materials may allow for more complex CPRs, providing a path to previously unexplored dynamical states. Utilizing graphene devices with local gates, one should be able to control the coupling strengths and to change the topology of the system at will. Finally, our observations may lend themselves useful as elements in superconducting microwave circuits. For example, the robust generation of down converted microwave photons, without the need for higher CPR harmonics, may allow for integrated on-chip applications in quantum information processing.

ASSOCIATED CONTENT

Supporting Information

The Supporting Information is available free of charge at https://pubs.acs.org/doi/10.1021/acs.nanolett.1c03474.

Further information about the studied sample, a discussion of the model, details of numerical simulations, and additional measurements studying frequency, temperature dependencies, and hysteresis (PDF)

AUTHOR INFORMATION

Corresponding Author

Ethan G. Arnault − *Department of Physics, Duke University, Durham, North Carolina 27708, United States;* orcid.org/0000-0002-9311-7624; Email: ethan.arnault@duke.edu

Authors

Trevyn F. Q. Larson − *Department of Physics, Duke University, Durham, North Carolina 27708, United States;* orcid.org/0000-0003-2441-3005

Andrew Seredinski − *Department of Physics, Duke University, Durham, North Carolina 27708, United States; School of Sciences and Humanities, Wentworth Institute of Technology, Boston, Massachusetts 02115, United States*

Lingfei Zhao − *Department of Physics, Duke University, Durham, North Carolina 27708, United States*

https://doi.org/10.1021/acs.nanolett.1c03474
Nano Lett. 2021, 21, 9668−9674

Sara Idris − *Department of Physics and Astronomy, Appalachian State University, Boone, North Carolina 28607, United States*
Aeron McConnell − *Department of Physics and Astronomy, Appalachian State University, Boone, North Carolina 28607, United States*
Kenji Watanabe − *Advanced Materials Laboratory, NIMS, Tsukuba 305-0044, Japan;* orcid.org/0000-0003-3701-8119
Takashi Taniguchi − *Advanced Materials Laboratory, NIMS, Tsukuba 305-0044, Japan;* orcid.org/0000-0002-1467-3105
Ivan Borzenets − *Department of Physics, City University of Hong Kong, Kowloon, Hong Kong SAR; Department of Physics and Astronomy, Texas A&M University, College Station, Texas 77843, United States;* orcid.org/0000-0002-1577-8312
François Amet − *Department of Physics and Astronomy, Appalachian State University, Boone, North Carolina 28607, United States*
Gleb Finkelstein − *Department of Physics, Duke University, Durham, North Carolina 27708, United States*

Complete contact information is available at: https://pubs.acs.org/10.1021/acs.nanolett.1c03474

Notes

The authors declare no competing financial interest.

■ ACKNOWLEDGMENTS

We thank Stephen Teitsworth and Michael Lee for helpful discussions. Transport measurements by E.G.A., F.A., and T.F.Q.L.; lithographic fabrication and characterization of the samples by E.G.A., F.A., A.S., and L.Z.; and data analysis by E.G.A., F.A., and G.F. were supported by Division of Materials Sciences and Engineering, Office of Basic Energy Sciences, U.S. Department of Energy, under Award No. DE-SC0002765. S.I. was supported by a GRAM fellowship. F.A. and A.M. were supported by a URC grant at Appalachian State University. K.W. and T.T. acknowledge support from JSPS KAKENHI grant number JP15K21722 and the Elemental Strategy Initiative conducted by the MEXT, Japan. T.T. acknowledges support from JSPS Grant-in-Aid for Scientific Research A (no. 26248061) and JSPS Innovative Areas "Nano Informatics" (no. 25106006). This work was performed in part at the Duke University Shared Materials Instrumentation Facility (SMIF), a member of the North Carolina Research Triangle Nanotechnology Network (RTNN), which is supported by the National Science Foundation (grant ECCS-1542015) as part of the National Nanotechnology Coordinated Infrastructure (NNCI). I.B. acknowledges CityU New Research Initiatives/Infrastructure Support from Central (APRC), 9610395, and the Hong Kong Research Grants Council (ECS) Projects (ECS) 2301818, (GRF) 11303619.

■ REFERENCES

(1) Stewart, W. Current-Voltage Characteristics of Josephson Junctions. *Appl. Phys. Lett.* **1968**, *12*, 277.
(2) McCumber, D. Effect of ac Impedance on dc Voltage-Current Characteristics of Superconductor Weak-Link Junctions. *J. Appl. Phys.* **1968**, *39*, 3113.
(3) Kautz, R. L. Noise, Chaos, and the Josephson Voltage Standard. *Rep. Prog. Phys.* **1996**, *59*, 935−992.
(4) Wiesenfeld, K.; Colet, P.; Strogatz, S. H. Synchronization Transitions in a Disordered Josephson Series Array. *Phys. Rev. Lett.* **1996**, *76*, 404−407.
(5) Abrams, D. M.; Strogatz, S. H. Chimera States for Coupled Oscillators. *Phys. Rev. Lett.* **2004**, *93*, 174102.
(6) Nichols, S.; Wiesenfeld, K. Ubiquitous neutral stability of splay-phase states. *Phys. Rev. A: At., Mol., Opt. Phys.* **1992**, *45*, 8430−8435.
(7) Strogatz, S. H.; Mirollo, R. E. Splay states in globally coupled Josephson arrays: Analytical prediction of Floquet multipliers. *Phys. Rev. E: Stat. Phys., Plasmas, Fluids, Relat. Interdiscip. Top.* **1993**, *47*, 220−227.
(8) Chung, J. S.; Lee, K. H.; Stroud, D. Dynamical properties of superconducting arrays. *Phys. Rev. B: Condens. Matter Mater. Phys.* **1989**, *40*, 6570−6580.
(9) Martinoli, P.; Leemann, C. Two Dimensional Josephson Junction Arrays. *J. Low Temp. Phys.* **2000**, *118*, 699−731.
(10) Tinkham, M. *Introduction to Superconductivity*; 2nd ed.; Dover, Mineola, NY, 1996; pp 210−214.
(11) Benz, S. P.; Rzchowski, M. S.; Tinkham, M.; Lobb, C. J. Fractional giant Shapiro steps and spatially correlated phase motion in 2D Josephson arrays. *Phys. Rev. Lett.* **1990**, *64*, 693−696.
(12) Riwar, R.-P.; Houzet, M.; Meyer, J. S.; Nazarov, Y. V. Multi-terminal Josephson junctions as topological matter. *Nat. Commun.* **2016**, *7*, 11167.
(13) Eriksson, E.; Riwar, R.-P.; Houzet, M.; Meyer, J. S.; Nazarov, Y. V. Topological transconductance quantization in a four-terminal Josephson junction. *Phys. Rev. B: Condens. Matter Mater. Phys.* **2017**, *95*, 075417.
(14) Meyer, J. S.; Houzet, M. Nontrivial Chern Numbers in Three-Terminal Josephson Junctions. *Phys. Rev. Lett.* **2017**, *119*, 136807.
(15) Xie, H.-Y.; Vavilov, M. G.; Levchenko, A. Topological Andreev bands in three-terminal Josephson junctions. *Phys. Rev. B: Condens. Matter Mater. Phys.* **2017**, *96*, 161406.
(16) Xie, H.-Y.; Vavilov, M. G.; Levchenko, A. Weyl nodes in Andreev spectra of multiterminal Josephson junctions: Chern numbers, conductances, and supercurrents. *Phys. Rev. B: Condens. Matter Mater. Phys.* **2018**, *97*, 035443.
(17) Nowak, M. P.; Wimmer, M.; Akhmerov, A. R. Supercurrent carried by nonequilibrium quasiparticles in a multiterminal Josephson junction. *Phys. Rev. B: Condens. Matter Mater. Phys.* **2019**, *99*, 075416.
(18) Fatemi, V.; Akhmerov, A. R.; Bretheau, L. Weyl Josephson circuits. *Phys. Rev. Research* **2021**, *3*, 013288.
(19) Peralta Gavensky, L.; Usaj, G.; Feinberg, D.; Balseiro, C. A. Berry curvature tomography and realization of topological Haldane model in driven three-terminal Josephson junctions. *Phys. Rev. B: Condens. Matter Mater. Phys.* **2018**, *97*, 220505.
(20) Venitucci, B.; Feinberg, D.; Mélin, R.; Douçot, B. Nonadiabatic Josephson current pumping by chiral microwave irradiation. *Phys. Rev. B: Condens. Matter Mater. Phys.* **2018**, *97*, 195423.
(21) Klees, R. L.; Rastelli, G.; Cuevas, J. C.; Belzig, W. Microwave Spectroscopy Reveals the Quantum Geometric Tensor of Topological Josephson Matter. *Phys. Rev. Lett.* **2020**, *124*, 197002.
(22) Pfeffer, A. H.; Duvauchelle, J. E.; Courtois, H.; Mélin, R.; Feinberg, D.; Lefloch, F. Subgap structure in the conductance of a three-terminal Josephson junction. *Phys. Rev. B: Condens. Matter Mater. Phys.* **2014**, *90*, 075401.
(23) Strambini, E.; D'Ambrosio, S.; Vischi, F.; Bergeret, F. S.; Nazarov, Y. V.; Giazotto, F. The ω-SQUIPT as a tool to phase-engineer Josephson topological materials. *Nat. Nanotechnol.* **2016**, *11*, 1055−1059.
(24) Cohen, Y.; Ronen, Y.; Kang, J.-H.; Heiblum, M.; Feinberg, D.; Mélin, R.; Shtrikman, H. Nonlocal supercurrent of quartets in a three-terminal Josephson junction. *Proc. Natl. Acad. Sci. U. S. A.* **2018**, *115*, 6991−6994.
(25) Draelos, A. W.; Wei, M.-T.; Seredinski, A.; Li, H.; Mehta, Y.; Watanabe, K.; Taniguchi, T.; Borzenets, I. V.; Amet, F.; Finkelstein, G. Supercurrent Flow in Multiterminal Graphene Josephson Junctions. *Nano Lett.* **2019**, *19*, 1039−1043.

(26) Pankratova, N.; Lee, H.; Kuzmin, R.; Wickramasinghe, K.; Mayer, W.; Yuan, J.; Vavilov, M. G.; Shabani, J.; Manucharyan, V. E. Multiterminal Josephson Effect. *Phys. Rev. X* **2020**, *10*, 031051.
(27) Graziano, G. V.; Lee, J. S.; Pendharkar, M.; Palmstrøm, C. J.; Pribiag, V. S. Transport studies in a gate-tunable three-terminal Josephson junction. *Phys. Rev. B: Condens. Matter Mater. Phys.* **2020**, *101*, 054510.
(28) Huang, K.-F.; Ronen, Y.; Mélin, R.; Feinberg, D.; Watanabe, K.; Taniguchi, T.; Kim, P. Interference of Cooper quartet Andreev bound states in a multi-terminal graphene-based Josephson junction. *arxiv.org*, 2020, 2008.03419, https://arxiv.org/abs/2008.03419 (accessed 8/8/2020).
(29) Josephson, B. D. Coupled Superconductors. *Rev. Mod. Phys.* **1964**, *36*, 216−220.
(30) Shapiro, S. Josephson Currents in Superconducting Tunneling: The Effect of Microwaves and Other Observations. *Phys. Rev. Lett.* **1963**, *11*, 80−82.
(31) Kwon, H.-J.; Yakovenko, V. M.; Sengupta, K. Fractional Ac Josephson Effect in Unconventional Superconductors. *Low Temp. Phys.* **2004**, *30*, 613−619.
(32) Fu, L.; Kane, C. L. Josephson Current and Noise at a Superconductor/Quantum-Spin-Hall-Insulator/Superconductor Junction. *Phys. Rev. B: Condens. Matter Mater. Phys.* **2009**, *79*, 161408.
(33) Rokhinson, L. P.; Liu, X.; Furdyna, J. K. The fractional a.c. Josephson effect in a semiconductor−superconductor nanowire as a signature of Majorana particles. *Nat. Phys.* **2012**, *8*, 795−799.
(34) Wiedenmann, J.; Bocquillon, E.; Deacon, R. S.; Hartinger, S.; Herrmann, O.; Klapwijk, T. M.; Maier, L.; Ames, C.; Brüne, C.; Gould, C.; Oiwa, A.; Ishibashi, K.; Tarucha, S.; Buhmann, H.; Molenkamp, L. W. 4π-periodic Josephson supercurrent in HgTe-based topological Josephson junctions. *Nat. Commun.* **2016**, *7*, 10303.
(35) De Cecco, A.; Le Calvez, K.; Sacépé, B.; Winkelmann, C. B.; Courtois, H. Interplay between electron overheating and ac Josephson effect. *Phys. Rev. B: Condens. Matter Mater. Phys.* **2016**, *93*, 180505.
(36) Picó-Cortés, J.; Domínguez, F.; Platero, G. Signatures of a 4π-periodic supercurrent in the voltage response of capacitively shunted topological Josephson junctions. *Phys. Rev. B: Condens. Matter Mater. Phys.* **2017**, *96*, 125438.
(37) Dean, C. R.; Young, A. F.; Meric, I.; Lee, C.; Wang, L.; Sorgenfrei, S.; Watanabe, K.; Taniguchi, T.; Kim, P.; Shepard, K. L.; Hone, J. Boron nitride substrates for high-quality graphene electronics. *Nat. Nanotechnol.* **2010**, *5*, 722−726.
(38) Mayorov, A. S.; Gorbachev, R. V.; Morozov, S. V.; Britnell, L.; Jalil, R.; Ponomarenko, L. A.; Blake, P.; Novoselov, K. S.; Watanabe, K.; Taniguchi, T.; Geim, A. K. Micrometer-Scale Ballistic Transport in Encapsulated Graphene at Room Temperature. *Nano Lett.* **2011**, *11*, 2396−2399.
(39) Borzenets, I. V.; Amet, F.; Ke, C. T.; Draelos, A. W.; Wei, M. T.; Seredinski, A.; Watanabe, K.; Taniguchi, T.; Bomze, Y.; Yamamoto, M.; Tarucha, S.; Finkelstein, G. Ballistic Graphene Josephson Junctions from the Short to the Long Junction Regimes. *Phys. Rev. Lett.* **2016**, *117*, 237002.
(40) Calado, V. E.; Goswami, S.; Nanda, G.; Diez, M.; Akhmerov, A. R.; Watanabe, K.; Taniguchi, T.; Klapwijk, T. M.; Vandersypen, L. M. K. Ballistic Josephson junctions in edge-contacted graphene. *Nat. Nanotechnol.* **2015**, *10*, 761−764.
(41) Ben Shalom, M.; Zhu, M. J.; Fal'ko, V. I.; Mishchenko, A.; Kretinin, A. V.; Novoselov, K. S.; Woods, C. R.; Watanabe, K.; Taniguchi, T.; Geim, A. K.; Prance, J. R. Quantum oscillations of the critical current and high-field superconducting proximity in ballistic graphene. *Nat. Phys.* **2016**, *12*, 318−322.
(42) Larson, T. F. Q.; Zhao, L.; Arnault, E. G.; Wei, M.-T.; Seredinski, A.; Li, H.; Watanabe, K.; Taniguchi, T.; Amet, F.; Finkelstein, G. Zero Crossing Steps and Anomalous Shapiro Maps in Graphene Josephson Junctions. *Nano Lett.* **2020**, *20*, 6998−7003.
(43) Lübbig, H.; Luther, H. Subharmonic steps in the I-V characteristic of short microbridges due to non-sinusoidal current-phase relations. *Rev. Phys. Appl.* **1974**, *9*, 29−34.
(44) Lee, G.; Kim, S.; Jhi, S.-H.; Lee, H.-J. Ultimately short ballistic vertical graphene Josephson junctions. *Nat. Commun.* **2015**, *6*, 6181.
(45) Snyder, R. A.; Trimble, C. J.; Rong, C. C.; Folkes, P. A.; Taylor, P. J.; Williams, J. R. Weak-link Josephson Junctions Made from Topological Crystalline Insulators. *Phys. Rev. Lett.* **2018**, *121*, 097701.
(46) Ueda, K.; Matsuo, S.; Kamata, H.; Sato, Y.; Takeshige, Y.; Li, K.; Samuelson, L.; Xu, H.; Tarucha, S. Evidence of half-integer Shapiro steps originated from nonsinusoidal current phase relation in a short ballistic InAs nanowire Josephson junction. *Phys. Rev. Research* **2020**, *2*, 033435.
(47) Bae, M.-H.; Dinsmore, R. C., III; Sahu, M.; Lee, H.-J.; Bezryadin, A. Zero-crossing Shapiro steps in high-T_c superconducting microstructures tailored by a focused ion beam. *Phys. Rev. B: Condens. Matter Mater. Phys.* **2008**, *77*, 144501.
(48) Dinsmore, R. C.; Bae, M.-H.; Bezryadin, A. Fractional order Shapiro steps in superconducting nanowires. *Appl. Phys. Lett.* **2008**, *93*, 192505.
(49) Sullivan, D. B.; Peterson, R. L.; Kose, V. E.; Zimmerman, J. E. Generation of Harmonics and Subharmonics of the Josephson Oscillation. *J. Appl. Phys.* **1970**, *41*, 4865−4873.
(50) Russer, P. Influence of Microwave Radiation on Current-Voltage Characteristic of Superconducting Weak Links. *J. Appl. Phys.* **1972**, *43*, 2008−2010.
(51) Valizadeh, A.; Kolahchi, M. R.; Straley, J. P. On the Origin of Fractional Shapiro Steps in Systems of Josephson Junctions with Few Degrees of Freedom. *Journal of Nonlinear Mathematical Physics* **2008**, *15*, 407−416.
(52) Panghotra, R.; Raes, B.; de Souza Silva, C.; Cools, I.; Keijers, W.; Scheerder, J.; Moshchalkov, V.; de Vondel, J. V. Giant fractional Shapiro steps in anisotropic Josephson junction arrays. *Nature Communications Physics* **2020**, *3*, 53.

https://doi.org/10.1021/acs.nanolett.1c03474
Nano Lett. 2021, 21, 9668−9674